

JGR Atmospheres

RESEARCH ARTICLE

10.1029/2020JD032695

Key Points:

- Homogenized 6.5- μm WV band radiance from GEO satellites is used for evaluating the monthly variation of UTWV nearly globally in reanalyses
- Reanalyses exhibit a dominant wet bias. ERA5, JRA55, and CRA are closer to the observations whereas MERRA-2 has the largest wet bias
- Reanalyses capture the pattern of UTWV well during the El Niño but underestimate the UTWV gradient over tropical Pacific in the decay year

Correspondence to:

J. Li,
 jun.li@ssec.wisc.edu

Citation:





Xue, Y., Li, J., Li, Z., Lu, R., Gunshor, M. M., Moeller, S. L., et al. (2020). Assessment of upper tropospheric water vapor monthly variation in reanalyses with near-global homogenized 6.5- μm radiances from geostationary satellites. *Journal of Geophysical Research: Atmospheres*, 125, e2020JD032695. <https://doi.org/10.1029/2020JD032695>

Received 29 FEB 2020

Accepted 28 JUL 2020

Accepted article online 1 SEP 2020

Assessment of Upper Tropospheric Water Vapor Monthly Variation in Reanalyses With Near-Global Homogenized 6.5- μm Radiances From Geostationary Satellites

Yunheng Xue^{1,2,3} , Jun Li² , Zhenglong Li² , Riyu Lu¹, Mathew M. Gunshor² ,
 Szuchia L. Moeller², Di Di⁴, and Timothy J. Schmit⁵ 

¹Institute of Atmospheric Physics, Chinese Academy of Sciences, Beijing, China, ²Cooperative Institute for Meteorological Satellite Studies, University of Wisconsin-Madison, Madison, WI, USA, ³College of Earth and Planetary Sciences, University of Chinese Academy of Sciences, Beijing, China, ⁴Key Laboratory for Aerosol-Cloud-Precipitation of China Meteorological Administration, School of Atmospheric Physics, Nanjing University of Information Science and Technology, Nanjing, China, ⁵NOAA/NESDIS/Center for Satellite Applications and Research, Madison, WI, USA

Abstract The monthly variation of upper tropospheric water vapor (UTWV) simulated by six reanalysis data sets is evaluated with homogenized water vapor radiance observations from international geostationary (GEO) weather satellites by using a profile-to-radiance approach over 45°N to 45°S regions for the period 2015–2017. Results show that reanalysis data sets have an overall good agreement with observations. However, a widespread wet bias is found in all reanalyses and is more dominant in large-scale subsidence regions. JRA55 has the smallest wet bias while MERRA-2 exhibits the most humid upper troposphere. The temporal variation of brightness temperatures in response to the warm phase of El Niño-Southern Oscillation (ENSO) in 2015–2016 indicates that the UTWV field is regulated by both ascending and descending branches of the large-scale circulation. All six reanalyses roughly capture the temporal variation of UTWV in the developing and decay year of this ENSO event. However, they tend to overestimate the eastward propagation of high UTWV in the developing year, especially MERRA-2. The UTWV gradient over the tropical Pacific in the decay year is underestimated, with a dry bias over the convective western Pacific and a wet bias over the eastern Pacific in reanalysis data sets. These results may provide a useful tool for the climate modeling community for identifying and solving problems associated with UTWV simulation.

1. Introduction

The upper tropospheric water vapor (UTWV) is an important indicator of large-scale atmospheric circulation and deep convective activities (Chung et al., 2011; Iacono et al., 2003; Luo et al., 2008; Schmetz & van de Berg, 1994). The high and low UTWV values are usually related with the ascending and descending branches of the Hadley cell and Walker circulations, respectively (van de Berg et al., 1991). Previous studies have demonstrated that the sensitivity of the outgoing longwave radiation (OLR) to changes in water vapor (WV) increases by more than 2 orders of magnitude from lower to upper troposphere (Schmetz, Geijo, et al., 1995; Schmetz, Menzel, et al., 1995). This indicates that the greenhouse effect is more sensitive to changes in upper tropospheric moisture. Therefore, even small changes of UTWV can have significant influence on the energy budget of the earth and play a key role in the climate feedback mechanism (Allan, 2012; Held & Soden, 2000; Houghton et al., 2001). However, UTWV is one of the most poorly understood atmospheric variables due to its small amount, high variability, and insufficient measurements (Elliott & Gaffen, 1991; Soden & Bretherton, 1993).

The climate reanalysis data sets are widely used for spatial-temporal variability analysis of key climate variables, detecting climate signals, and evaluation of numerical models (Davis et al., 2017; Dessler & Davis, 2010; Jiang et al., 2015; Ren et al., 2017; Shangquan et al., 2019; Trenberth et al., 2011). The reanalysis is based on a state-of-the-art numerical weather prediction (NWP) model with the assimilation of multiple in situ and remotely sensed observations. However, the assimilation of humidity fields in reanalysis data might be problematic in the upper troposphere and above, where WV concentrations are very small and valid observations are very sparse (Fujiwara et al., 2017; Iacono et al., 2003; Jiang et al., 2015). Therefore, the

assimilations might be absent in these regions, and thus, the reanalysis heavily relies on the dynamics and physics of its host model. Early studies have shown that UTWV in different reanalysis data sets can be significantly different (Chuang et al., 2010; Dessler & Davis, 2010). Given the importance of UTWV for radiative forcing and climate feedback, small UTWV biases in reanalysis data sets may cause non-negligible radiative and dynamical impacts. Besides, the inappropriate representation of UTWV usually means unsuitable parameterization of deep convection, insufficient data assimilation, and inadequate representation of large-scale circulations in reanalysis data sets (Brogniez & Pierrehumbert, 2006; Gregory, 1997; Takahashi et al., 2016). Therefore, it is important to assess whether reanalysis data sets can reproduce the observed distribution and variability of UTWV on various time scales.

Unfortunately, there is a lack of accurate global-scale UTWV observations. Conventional observations such as those from radiosonde and aircraft have large spatial and temporal gaps. They are also reported to have large biases in the upper troposphere (Elliott & Gaffen, 1991; Miloshevich et al., 2006; Wang et al., 2003). The limitations of in situ measurements facilitate the use of remotely sensed satellite observations in the WV absorption band (most notably the infrared [IR] 6.0- to 7.0- μm band). Currently, Low Earth Orbiting (LEO) satellites and geostationary (GEO) satellites collect data from that spectral region. Early studies have used the humidity retrievals from satellite radiances to investigate the variability of upper tropospheric relative humidity (UTH) and examine the model simulations (Bates & Jackson, 1997; John & Soden, 2007; Pierce et al., 2006). Recently, studies have attempted to assess the quality of UTWV in general circulation models (GCMs) and reanalysis data sets directly using the WV radiances from both LEO and GEO satellites. As shown by Soden and Bretherton (1993), the IR radiance from around 6.7- μm channels is primarily sensitive to the WV averaged over a deep layer typically between 200 and 500 hPa and thus can be used to accurately infer the UTWV (Brogniez et al., 2006; Tian et al., 2004). For example, Chung et al. (2013) have used the Meteosat WV clear-sky radiances from Brogniez et al. (2006) to assess the diurnal cycle of UTH in five reanalysis data sets for the period of 1984–2004 over the convectively active regions of Africa and the Atlantic Ocean. Iacono et al. (2003) have evaluated the monthly and 5-day mean UTWV simulated by the National Center for Atmospheric Research (NCAR) Community Climate Model (CCM3) by using the 6.7- μm WV band from High-Resolution Infrared Radiation Sounder (HIRS). Similarly, a study by Chung et al. (2011) has assessed the Geophysical Fluid Dynamics Laboratory (GFDL) climate model and ERA-40 reanalysis using long-term mean 6.7- μm radiances from HIRS. However, these studies are usually limited to LEO satellites, which only provide full global coverage twice a day. Although some studies have used GEO satellites with higher temporal sampling, they used only a single satellite due to the spectral differences among international GEO satellites. Therefore, these studies were usually confined to some local areas.

In a recent study, a new data set (Li et al., 2019) providing consistent IR 6.5- μm WV absorption band radiances from international GEO satellites (referred to as homogenized WV radiances data in this paper) has been successfully generated and validated with hyperspectral sounder (Menzel et al., 2018) Infrared Atmospheric Sounding Interferometer (IASI) radiances. This data set incorporates multiple GEO imagers from international agencies (such as NOAA, EUMETSAT, and JMA). Therefore, this homogenized WV radiances data set maintains the high spatial and temporal resolution of GEO satellites and has near global coverage. More information about this data set is given in section 2. It offers a great opportunity to assess the ability of climate reanalysis to simulate global UTWV on various time scales. For example, Xue et al. (2020) have demonstrated an evaluation study of the diurnal variations of upper tropospheric moisture simulated in five reanalysis data sets using the homogenized WV radiances data. They found that reanalysis can roughly reproduce the day-night contrast of UTH but with much weaker amplitudes and later peak time over both land and ocean. The monthly variation is one of the most fundamental modes of variability of the global climate system. Analysis of the monthly mean UTWV helps to provide insight into the investigations of longer time variations and the related climate processes like El Niño-Southern Oscillation (ENSO). One important application of reanalysis data sets is to study the long-term variations of atmospheric variables. Within this context, a global, comprehensive, and unambiguous assessment of the monthly mean UTWV simulated in modern reanalysis data sets is especially important. In this study, six global atmospheric reanalysis data sets from the world's major meteorological centers (ECMWF, NCEP, NASA, JMA, and CMA) are evaluated using the homogenized WV radiances data set from 2015 to 2017 to reveal their similarities and differences in the variation of monthly mean UTWV. The period of 2015–2017 is selected because the homogenized GEO WV radiances are currently processed and validated with IASI for these three years. This

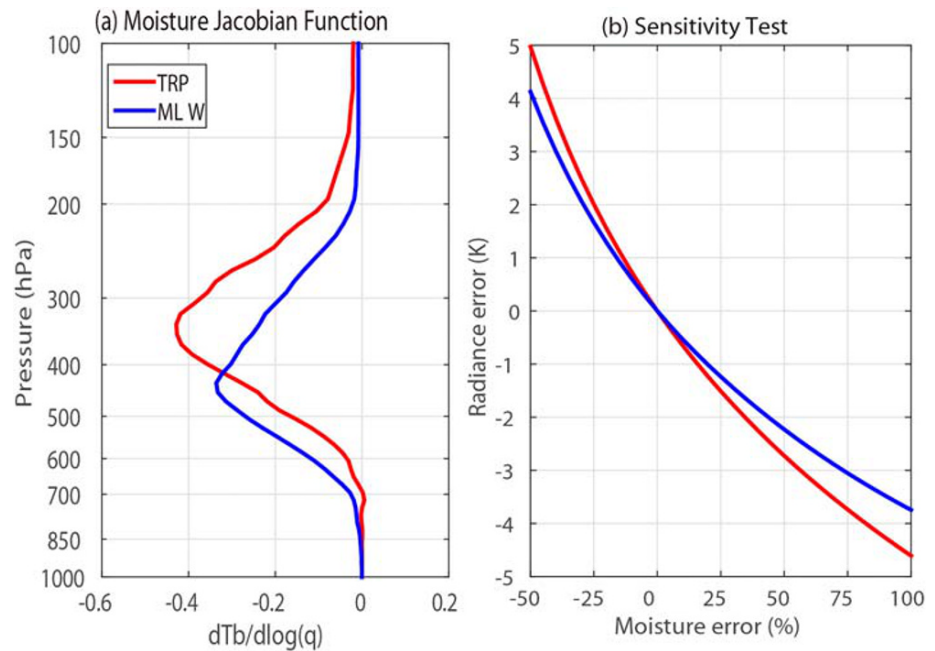


Figure 1. (a) Moisture Jacobian function of the GOES-15 Imager 6.5- μm WV band and (b) the radiance sensitivity to moisture uncertainty of the whole troposphere for standard TRP and MLW profiles with a nadir view.

period also includes a strong 2015–2016 El Niño and a transition to weak La Niña during 2016–2017 that allows the evaluation to be performed over a wide range of atmospheric conditions.

It is noteworthy that some of these satellite observations have been assimilated by the reanalysis data sets. Although the evaluation should ideally use independent observations, this is not always possible especially for reanalysis data sets, which are generated from DA systems with almost all available observations, especially satellite observations, assimilated. However, the proportion of assimilated satellite observations, especially the WV information, is rather small due to thinning strategies, channel selection, and quality control checks (O-B check, error inflation, etc.) in DA systems. Additionally, the assimilation of satellite observations is usually absent in the upper troposphere and above in reanalysis data, and the WV field is typically determined by their forecast model alone (Fujiwara et al., 2017). Therefore, the homogenized WV radiances data set remains an important and independent tool for the evaluation of reanalysis data sets and especially in the upper troposphere.

The data sets and methodologies are described in section 2. Section 3 compares the variation of UTWV between simulated and observed WV radiances. Conclusions and discussions are provided in section 4.

2. Data and Methodologies

2.1. Radiance Observations From International GEO Weather Satellites

The reference data used in this study are homogenized clear-sky IR radiances (expressed as equivalent brightness temperatures [BTs]) in the 6.5- μm WV absorption band from seven imagers onboard international GEO weather satellites, including GOES-13 Imager (G13I), G15I, ABI16, AHI8, MTSAT-2, and Meteosat-8/Meteosat-10 SEVIRI (SEVIRI08 and SEVIRI10) (see Table 1 in Li et al., 2019). It covers the years from 2015 to 2017 at the temporal resolution of 3 hr over the latitudes of 45°N to 45°S and all longitudes. Only a few essential facts about this homogenized WV radiances data set are given here for completeness; the reader is referred to Li et al. (2019) for detailed technical approaches. This data set was generated by homogenizing all other GEO Imager WV radiances to the nadir view radiances of GOES-15 Imager 6.5- μm WV band. The process accounts for both the limb effect and the spectral differences among different GEO imagers. Since the clear-sky 6.5- μm BTs are contaminated in the presence of high clouds (Brogniez et al., 2006; Chung et al., 2011), a simple cloud mask scheme was applied in postprocessing to remove

those contaminated pixels. Then the accuracies of the homogenized WV radiances are validated with independent data from the high spectral resolution IASI radiances from both Metop-A and Metop-B. The results show that all the clear-sky WV radiances are homogenized well, with small standard deviations (STDs) and biases (mostly smaller than 0.2 K) of the differences and with temporally stable radiometric accuracy.

Figure 1 illustrates the sensitivity of BTs from 6.5- μm band to WV changes in the troposphere using clear-sky standard tropical (TRP) and midlatitude winter (MLW) profiles to represent different atmospheric states. The moisture Jacobian function of this band is shown in Figure 1a. The moisture Jacobian function is defined as the variation of the radiance for a specific band in response to the unit perturbation of WV at each pressure level. It provides the best water vapor information layer (BWIL), that is, the atmospheric pressure layer at which the measured radiance was most sensitive to the WV changes (Di et al., 2016). Figure 1a shows that the BWIL of the 6.5- μm WV absorption band is a broad layer centered in the upper troposphere roughly between 200 and 600 hPa, which means that the changes of the clear-sky 6.5- μm WV BTs can be interpreted as changes in the vertically averaged moisture approximately between 200 and 600 hPa. The BWIL is higher in tropical areas than in midlatitude regions due to the higher WV content in TRP profiles. Figure 1b further provides the quantitative relationship between the 6.5- μm radiance error and moisture error. It demonstrates that the 6.5- μm BT change is nearly proportional to the natural logarithm of the WV change. A decrease (increase) in BT corresponds to an increase (decrease) in WV in the upper troposphere. This was also illustrated by Soden and Bretherton (1993), and they found that this simple radiance-to-humidity relationship explains greater than 90% of the variability in BT for WV channels, indicating that the humidity has substantially greater influences on BT variation in comparison to temperature. Moreover, Figure 1b shows that a 70% relative moisture increase will cause a 3.7 K (3.0 K) of BT decrease for TRP (MLW) profiles. This large BT difference (BTD) would need an equivalent temperature difference of 3.7 K (3.0 K) in TRP (MLW) profiles, which is unlikely for the troposphere in current reanalysis data sets. Actually, previous studies have found that the upper troposphere temperature error in reanalysis data is within 0.3 K when compared with microwave sounder unit (MSU) observations (Santer et al., 2003; Trenberth et al., 2001). Therefore, large differences between observations and reanalysis simulations could be primarily attributed to the moisture uncertainties in reanalysis data sets. In other words, these homogenized 6.5- μm WV band radiance observations with near global coverage can be used to evaluate the UTWV in reanalysis data sets directly and effectively.

2.2. Overview of Six Reanalysis Data Sets

The six reanalysis data sets evaluated in this study are the European Centre for Medium-Range Weather Forecasts (ECMWF) Interim Reanalysis (ERA-Interim; Dee et al., 2011), the newly released fifth-generation ECMWF reanalysis (ERA5; Hersbach & Dee, 2016), the National Centers for Environmental Prediction (NCEP) Climate Forecast System, version 2 (CFSv2; Saha et al., 2014) reanalysis, the Modern-Era Retrospective Analysis for Research and Applications version 2 (MERRA-2; Gelaro et al., 2017), the 55-year modern Japanese Reanalysis Projects (JRA55; Kobayashi et al., 2015), and the newly developed China Meteorological Administration (CMA) reanalysis (CRA; Jiang et al., 2018). Table 1 summarizes some basic characteristics of the six climate reanalysis data sets in this assessment. Some highlights are also given below.

ERA5 is the latest global reanalysis from ECMWF, which was released in 2017 and will replace ERA-Interim eventually. The horizontal ($0.25^\circ \times 0.25^\circ$) and temporal resolution (1 hr) of ERA5 is significantly improved compared with that in ERA-Interim. Another improvement is the upgraded DA system from Cycle 31r2 to 41r2 of the Integrated Forecasting System (IFS) with a four-dimensional variational analysis (4-D-Var). ERA5 benefits from the developments of model physics, dynamics schemes, and DA systems that allow more observations to be ingested. CFSv2 reanalysis used the NCEP CFSv2 analysis system which was made operational in 2011. The DA system used was the Gridpoint Statistical Interpolation (GSI), with 3-D-Var. Because CFSv2 reanalysis was intended as the continuation of CFSR, in this paper it is referred to as CFSR directly.

MERRA-2, released in 2015, is a follow-on project of MERRA by NASA's Global Modeling and Assimilation Office (GMAO). It is produced with a recently developed Goddard Earth Observing System-5 (GEOS-5) atmospheric general circulation model (AGCM), together with the GSI analysis scheme with 3-D-Var. MERRA-2 has some substantial improvements in the forecast model, DA system, and input data compared with MERRA. A major change related with WV is that a series of new constraints are applied to ensure the

Table 1
Basic Characteristics of Reanalysis Data Sets Evaluated in This Paper

Reanalysis	Source	Time span	Assimilation scheme	Vertical resolution (pressure level)	Horizontal resolution	Temporal resolution
ERA5	ECMWF	1950 to present	4-D-Var	37	$0.25^\circ \times 0.25^\circ$	1 hourly
ERA-Interim	ECMWF	1979 to present	4-D-Var	37	$0.75^\circ \times 0.75^\circ$	6 hourly
CFSR	NCEP	2011 to present	3-D-Var	37	$0.5^\circ \times 0.5^\circ$	6 hourly
MERRA-2	NASA GMAO	1980 to present	3-D-Var	42	$0.5^\circ \times 0.625^\circ$	3 hourly
JRA-55	JMA	1958 to present	4-D-Var	37; 27 for WV profiles	$1.25^\circ \times 1.25^\circ$	6 hourly
CRA	CMA	2007–2016 ^a	3-D-Var	47	$0.3125^\circ \times 0.3125^\circ$	6 hourly

^aThe complete CRA-40 data set spanning the period from 1979 to near real time is ongoing.

continuity of water mass in the atmosphere (Takacs et al., 2016). The highest level of assimilated WV observations for MERRA-2 is 300 hPa whereas it is 100 hPa for JRA-55, another global reanalysis released in 2013 by JMA. JRA-55 was extensively improved compared with the earlier Japanese 25-year Reanalysis (JRA-25) and was produced by the TL319 version of JMA's operational DA system, which now includes 4-D-Var. Moreover, JRA-55 sets the vertical correlations of humidity background errors to zero at pressures smaller than 5 hPa in case of the spurious analysis increments at higher levels and only provides WV profiles below 100 hPa in the pressure-level analysis products. CRA is a reanalysis project started by CMA since early 2014 aiming at producing its first-generation 40-year (1979–2018) global atmospheric and land reanalysis data. Recently, a 10-year interim product (CRA-Interim, 2007–2016, referred as CRA hereafter) was completed. The most notable feature of this reanalysis is the assimilation of more observations over China.

2.3. Methodologies

This evaluation is based on homogenized WV radiances rather than on retrievals from international GEO weather satellites. To be consistent with the homogenized WV radiance data, the atmospheric profiles of temperature and humidity with some surface information from reanalysis data sets in their original resolution were input into a radiative transfer model to simulate the clear-sky $6.5\text{-}\mu\text{m}$ WV band BTs at nadir view. The model used is the Community Radiative Transfer Model (CRTM) v2.1.3 using Optical Depth in Pressure Space (ODPS) coefficients, which is designed to provide reasonable radiance simulations from a variety of sensors and instruments (Han, 2006). This approach is computationally efficient and more accurate than attempting to retrieve WV amounts from WV band radiances. Since reanalysis data sets and satellite observations have different spatial resolutions, they are all first regridded to a $0.5^\circ \times 0.5^\circ$ horizontal grid resolution using an inverse distance squared weighted interpolation method. For observations, the value is only calculated with a minimum of 10% clear-sky pixels in a $0.5^\circ \times 0.5^\circ$ grid box; otherwise, the value on that grid will be discarded. To avoid spatial sampling differences over cloudy areas between observations and simulations as a result of the assumption of no clouds in CRTM simulations using all profiles from reanalysis data sets, a simple cloud detection procedure based on gridded clear-sky observations is used for reanalysis data sets. Specifically, the simulations from reanalysis are sampled onto the same gridded clear-sky satellite observations to exclude the reanalysis grids that are observed cloudy by GEO satellites. Soden and Bretherton (1994) have provided a rough estimate of the bias introduced by including model simulations on all grids in comparisons to clear-sky only grids. The difference in monthly mean BTs for different areas is always less than 0.52 K. Therefore, remaining uncertainties caused by the possible high cloud contamination in reanalysis for the same spatial sampling will be much smaller than 0.5 K. More discussions will be provided in the following comparison results.

The comparisons are based on monthly or longer time averaged gridded data; thus, both random noise in BT observations and CRTM calculations will be significantly reduced, and differences between observations and simulations for the same period can be mainly attributed to moisture differences in the upper troposphere. The bias, STD, root mean square error (RMSE), probability density function (PDF), and a PDF skill score (Mao et al., 2010; Maxino et al., 2008) are calculated for comparisons. The PDF skill score is the cumulative minimum value of each binned value in two PDFs measuring their common area. It is a very simple way to provide an overall measure of the similarity between reanalysis simulated and satellite observed

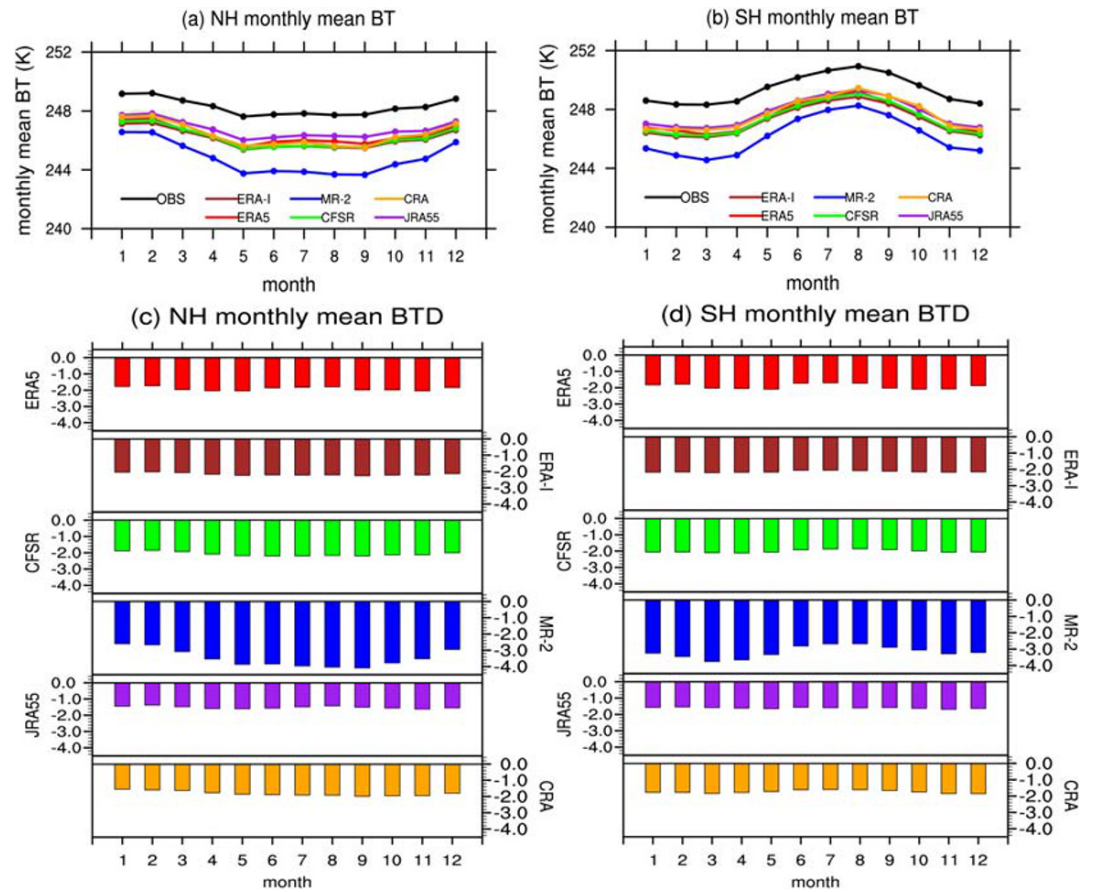


Figure 2. Seasonal cycle of area-weighted mean BTs for the (a) northern and (b) southern hemispheres, and BTDs (reanalyses minus observations) for the (c) northern and (d) southern hemispheres in 2015–2017. The northern hemisphere (NH) is 0–45°N, and the southern hemisphere (SH) is 0–45°S. The BT variation from observations is indicated by the black line. The BT variations from ERA5, ERA-Interim, JRA55, and CRA are shown by lines with colors of red, brown, green, blue, purple, and orange, respectively. The BTDs are denoted by the bar chart with corresponding colors. Units are in degrees K. ERA-I is short for ERA-Interim, and MR-2 is short for MERRA-2, hereafter in all figures.

distributions of BTs. The higher the skill score is, the more similar the two PDFs are. If the reanalysis simulates observations perfectly, the skill score will equal one.

3. Comparisons Between Simulated and Observed BTs

3.1. Annual Cycle

Figure 2 shows the seasonal cycle of the area-weighted average of observed and simulated BTs over the northern (0–45°N) and southern (0–45°S) hemisphere for the three years. The weights were calculated by taking the cosine of the latitude. The area-weighted average method is more reasonable than uniform average in the global analysis and has been used in a wide range of research contexts (Iacono et al., 2003; Lavers et al., 2015; Xue et al., 2019). Cold (warm) BTs indicate more (less) WV absorption in the upper troposphere, and thus, the radiation to space is emitted from higher levels (where it is colder). As expected, colder BTs are found in wet summer with warmer BTs in dry winter, which again proved that the moisture content is the dominant factor of nadir 6.5- μm BTs. The phase of BT variations in six reanalysis data sets agrees well with observations. Differences among reanalysis data sets themselves are small except the MERRA-2. However, the magnitudes of simulated BTs are smaller in all reanalysis data sets than the observed ones, which means that all reanalyses overestimate the monthly mean UTWV throughout the whole year. The bar chart of BTDs defined as simulated BTs minus observed BTs is also provided (Figures 2c and 2d). Negative BTDs represent

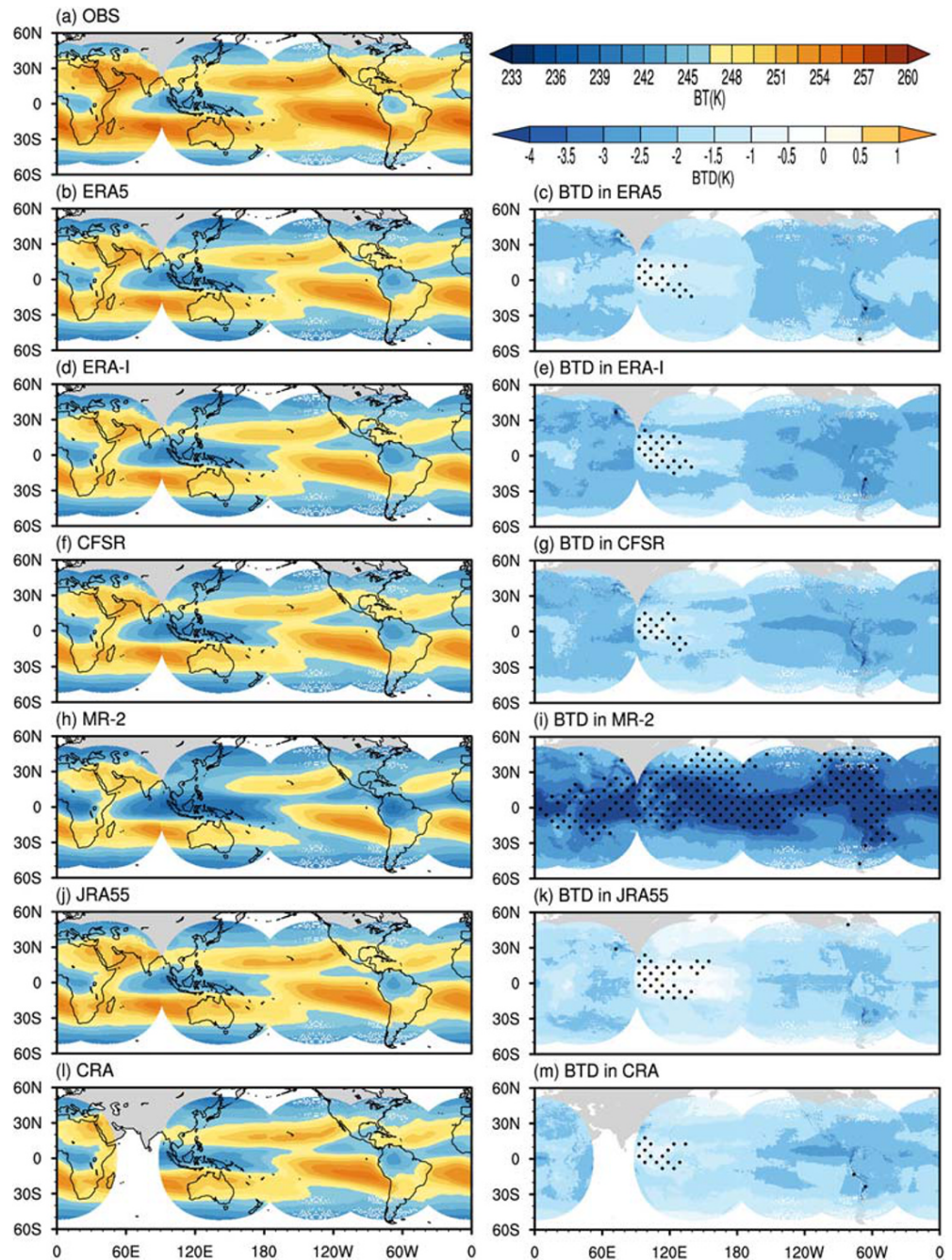


Figure 3. The distributions of BTs (left panel) and BTDs (right panel) from observations and reanalysis simulations in 2015–2017. The STD of monthly mean BTD (in these three years) larger than 0.75 K is stippled black in the BTD figure.

colder BTs in reanalyses than observations and correspond to wet biases in the upper troposphere in reanalysis data sets, while positive BTDs indicate dry biases. JRA55 has the smallest mean BTD of about -1.5 K whereas MERRA-2 has the largest bias with a mean BTD of -3.5 K in both hemispheres. As inferred from Figure 1b, this range of BTDs is corresponding to a relative moist error from 25% up to 85% in comparison to observations. It is also shown that the BTD in MERRA-2 has an obvious seasonal variation consistent with the seasonal migration of the intertropical convergence zone (ITCZ), and the largest error occurs in the summer (wet) hemisphere. However, this seasonal variation of BTDs is not obvious in other reanalysis data sets.

Table 2
Statistical Results of 3-Year Mean BTDs in Six Reanalysis Data Sets in 2015–2017

Unit (K)	Reanalysis					
	ERA5	ERA-Interim	CFSR	MERRA-2	JRA55	CRA
Mean bias	−1.92	−2.17	−2.06	−3.36	−1.57	−1.77
RMSE	1.95	2.20	2.09	3.46	1.65	1.82

3.2. Global Distributions

The spatial distributions of the 3-year mean BTs (left panel) and the BTDs (right panel) between reanalyses and observations for 2015–2017 are shown in Figure 3. It should be noted that CRA is only available for the year of 2015–2016, so all comparisons related to CRA are referred to observations in the same periods. Additionally, observations from Meteosat-8 included in the homogenized WV radiances data set are only available since November 2016. Therefore, there is a lack of data over the Indian Ocean until then, which is more obvious in CRA data.

As shown in Figure 3a, the geographic distributions of BTs are smooth in overlap regions between different satellites, which further indicates that this homogenized WV radiances data set has good performance regarding homogeneity and consistency. Another prominent characteristic is the zonal distribution of BTs throughout the globe. This zonal pattern reflects that the mean distribution of UTWV could be highly influenced by large-scale circulations such as the Hadley circulation. In general, the simulated BTs in different reanalysis data sets are in good agreement with observations in terms of geographic patterns. This indicates the reanalysis data sets, through continuous assimilation of observations, are able to capture the main signals of UTWV, as where UTWV is abundant (cold BT) or sparse (warm BT). The BTs colder than 246 K correspond to moist regions where convections are more active, such as the Indo-Pacific warm pool including the maritime continent, north of South America, and tropical Africa. In these regions, strong convective updrafts bring sufficient moisture to the upper troposphere and finally lead to colder BTs. Previous studies (Basha et al., 2013; Zhan et al., 2006) have also found that convection is the main driving force of the UTWV. Monsoonal circulations in monsoon seasons can contribute up to 75% of the upward WV at tropopause levels.

The dry zones with warm BTs are also well defined over both hemispheres. The warmer BT band is stronger over the southern subtropics, ranges from the eastern Pacific Ocean, stretching across South America, the Atlantic Ocean, and Southern Africa into Oceania, with the maximum values centered over open oceans off the west coast of continents. By contrast, the warm BT band in the northern subtropics is slightly weaker, with large values found over the central Pacific, the tropical Atlantic, and all the way to Arabia and the Indian subcontinent. The symmetry bands of warm BTs in the subtropics of both hemispheres correspond to the dominant descending branches of the global-scale Hadley circulation in these areas. Additionally, the asymmetry distribution of cold and warm BTs over the tropical Pacific reveals the Walker circulation, which brings the moisture to the western Pacific and the dry air to the eastern Pacific. Overall, six reanalysis data sets have similar global distributions of BTs (UTWV) as the observations, and the locations of convective centers and dry zones are reproduced well. However, it is shown that reanalysis data sets overestimate the range of colder BTs, especially in MERRA-2, indicating more WV in the upper troposphere. On the other hand, the range and magnitude of warm BT zones in six reanalysis data sets are underestimated, which means less UTWV in reanalysis data sets compared with observations in these regions.

The spatial distributions of BTDs clearly show that all reanalysis data sets have a worldwide cold bias with area-weighted averages ranging from −1.57 to −3.36 K, which represents an overall wet bias of about 25% to 85% in the upper troposphere (Figure 1b). The statistical results of the error analysis are listed in Table 2. Among all six reanalysis data sets, JRA55 has the smallest bias with the area-weighted average BTD of −1.57 K, followed by CRA with an average error of −1.77 K, and then ERA5 of −1.92 K. The largest bias is found in MERRA-2 with an average BTD of −3.36 K. According to Figure 1b, this BTD is equivalent to a moisture error in the upper troposphere of about 65% in the tropics and 85% in the midlatitudes. Some studies (Chung et al., 2011; Jiang et al., 2015) have emphasized that the UTWV bias is strongly affected by the bias in the large-scale circulation. Therefore, the prevalent moist biases in Figure 3 may suggest that the

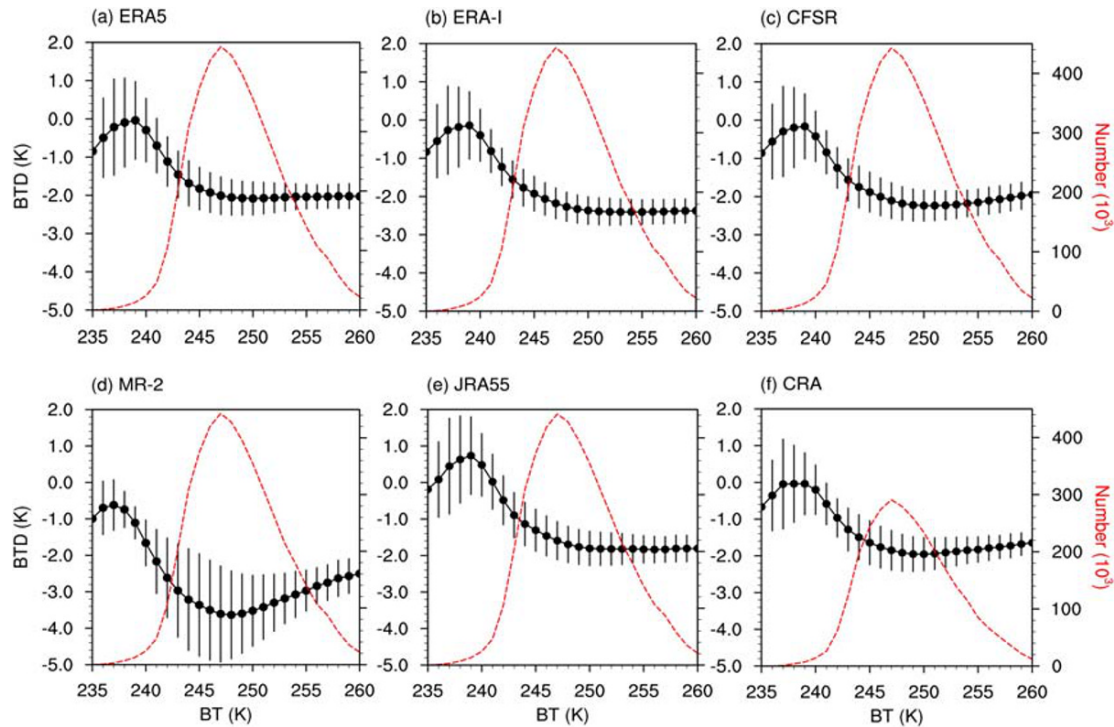


Figure 4. The mean and STD of the monthly BTDs from reanalysis data sets as a function of monthly mean BTs from observations in 2015–2017. The number of observed BTs in each interval is denoted by the red dashed line with the unit of 1,000. Note that the number of observations in CRA is only for 2015–2016.

large-scale circulation in reanalysis data is not well simulated. The regions where the STD of monthly mean BTD in these three years is larger than 0.75 K are highlighted with black stipples in Figure 3. Although the 3-year mean BTDs are smaller over the maritime continent and western Pacific in reanalysis data sets, except MERRA-2, the larger STDs imply that the BTDs in these areas have larger temporal variations. In MERRA-2, the wide zonal belts with larger STDs are consistent with the tracks of ITCZ movements indicating the high correlation between the BTD variations and deep convection activities in MERRA-2, which is also reflected in Figure 2. Jiang et al. (2015) have found that MERRA-2 produces much faster vertical WV transport velocities across the tropical upper troposphere and larger horizontal transport speed ratios out of the monsoon convection than Aura Microwave Limb Sounder (MLS) observations. This may contribute to the pronounced wet biases in MERRA-2.

It is interesting to see some discontinuities between different sensors on the BTD figures. These small magnitude discontinuities are not visible on the observed and simulated BTs on the left panel of Figure 3. They are caused by different levels of residual bias from different sensors in the homogenized WV data set. For example, from Figure 3 of Li et al. (2019), the seven GEO imagers have overall biases ranging from -0.149 to -0.365 K. Also, the bias magnitudes increase with local zenith angle. So the discontinuities are most visible along the full disk edge because that's where one of the sensors has the largest bias. However, the magnitudes of these discontinuities are mostly smaller than 0.2 K, much smaller than the 3-year mean BTD. Thus, they will not affect the discussion above.

While Figure 3 shows that all reanalysis data sets have wet biases (negative BTDs), it appears that wet regions (with cold BTs) have smaller wet biases in absolute value. To investigate that, the mean and STD of monthly BTDs are calculated in 1-K intervals of observed BTs in Figure 4, together with the number of BTs at each interval indicated by the red dashed line. It is clear that when observed BTs are smaller than 242 K (high UTWV), the wet biases are not as large. It is even possible to find dry biases in reanalysis data sets, that is, JRA55 for BTs of 236 to 241 K. While the sample size of observed BTs below 242 K is relatively small, it does indicate that the wet conditions are not in favor of wet biases in reanalysis data. As the upper troposphere gets drier, the wet bias becomes more significant. The large wet biases are dominant over the

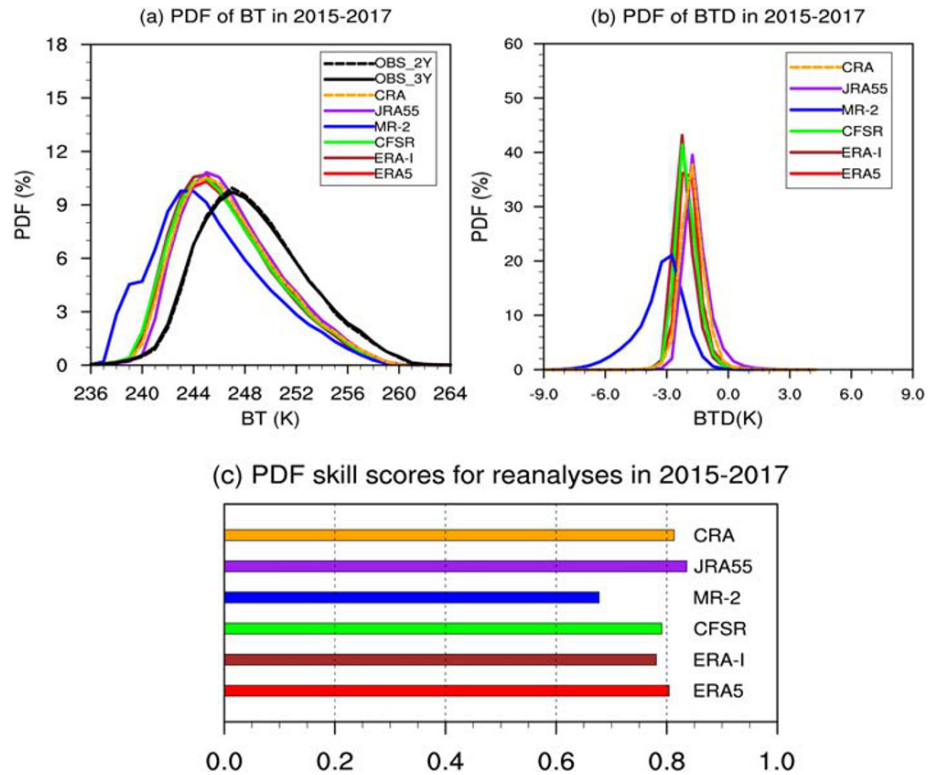


Figure 5. The probability density function (PDF) of monthly mean (a) BTs and (b) BTDs from observed and reanalysis data sets in 2015–2017, together with the (c) PDF skill score for each reanalysis.

large-scale subsidence zones where the BTs are larger than ~245 K (Figure 3). Takahashi et al. (2016) found that Coupled Model Intercomparison Project Phase 5 (CMIP5) models tend to have moist biases over the large-scale descending regimes. They referred to Su et al. (2013) to attribute the bias to the underestimation of the vertical velocity at 500 hPa in CMIP5 models over descending regimes. Similarly, the results here suggest that the reanalysis models may underestimate the intensity of large-scale descending branches, resulting in excessive wet biases. Figure 4 also shows that all reanalysis data sets show relatively flat wet biases for BTs greater than 245 K except MERRA-2. In addition, MERRA-2 has the largest STD for BTs around 245 K, indicating that MERRA-2 has difficulty simulating the temporal variations in intermediate wet/dry conditions. The other five data sets show the largest STD around wet conditions. This is probably more reasonable because wet conditions are more associated with deep convections, which are more temporally variable and more difficult to simulate. Overall, the distribution and STD of the BTDs are similar in all reanalysis data sets except MERRA-2. While MERRA-2 appears to simulate the wet conditions well, it has the largest STD of BTDs within 245–250 K of BTs, which is much larger than other reanalysis data sets. The reason for this may need further investigation into the host forecast models of MERRA-2.

It might be questioned that the moist bias found in reanalysis data sets is induced by cloud contamination in reanalysis simulations. However, as shown by Figures 3 and 4, the moist biases are more dominant over the wide subtropical dry regions (warm BTs) where high clouds are rare, and the clear/cloudy sampling biases are not important (Soden & Bretherton, 1994). In comparison, reanalyses tend to have smaller wet biases or even dry biases over deep convection regions with cold BTs (e.g., western Pacific warm pool) where the cloud contamination in reanalysis is likely to be the largest and reanalysis should have larger wet biases. Therefore, the cloud contamination cannot explain the observed pattern of the BTDs especially over the warm BT regions. Similarly, Chung et al. (2011) also found that the clear/cloudy sky bias is not remarkable over the majority of the tropics and subtropics.

The PDF analysis will give the probabilities of occurrence of BTs and BTDs in each bin and not smear out the differences caused by spatial averaging. Therefore, it provides an overall impression of the performance of

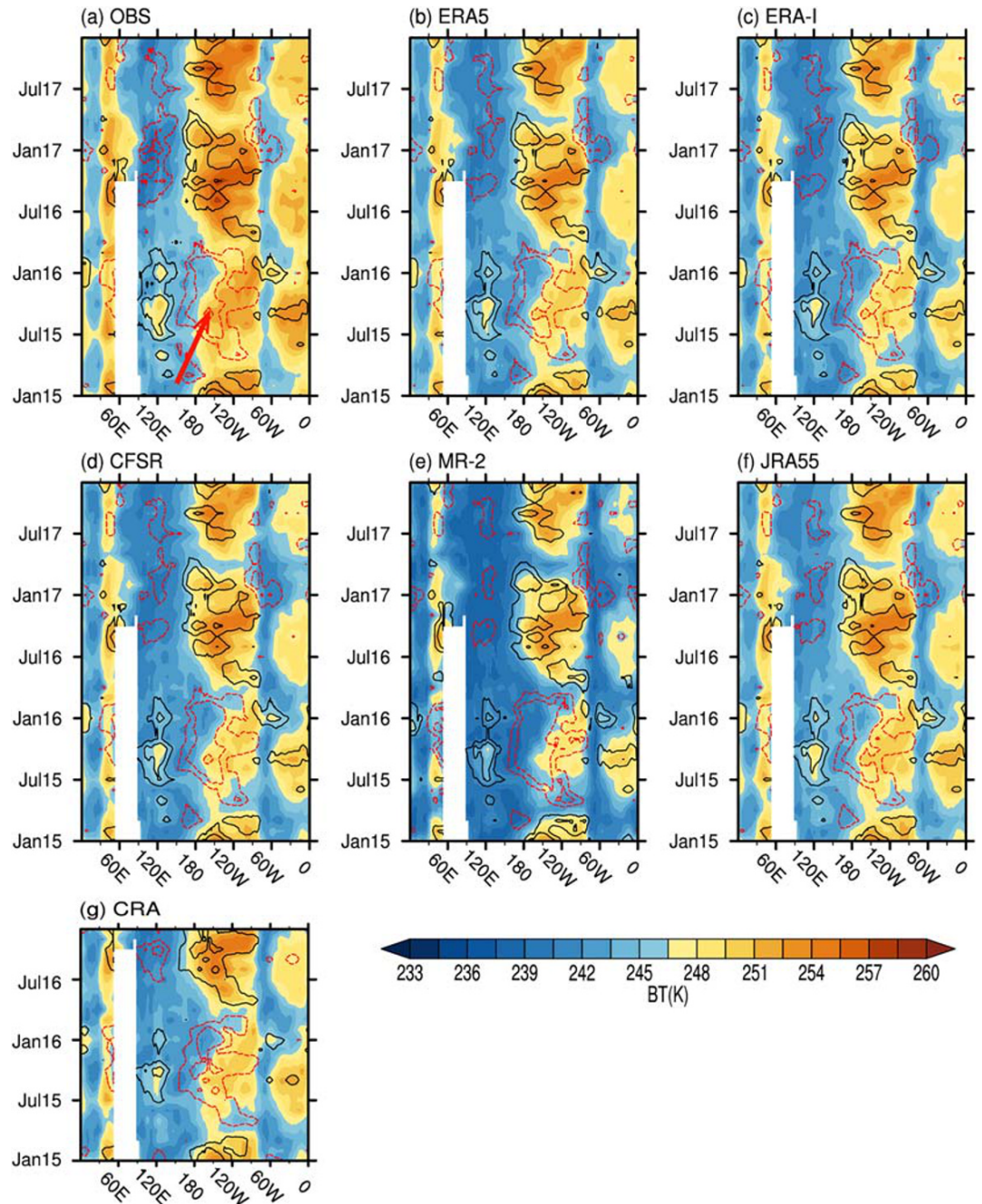


Figure 6. Hovmöller diagrams of the (shaded) monthly mean BTs and (contours) monthly anomalies of BT averaged over 5°N to 5°S in the observed and reanalysis data sets for 2015–2017. Contours are drawn every 1.5 K with the positive anomalies in black, negative anomalies in red, and the zero-contour omitted. The solid red arrow represents the eastward propagation of the centers of negative anomalies during 2015. The white colored area is due to the missing data in this region caused by the limited availability of observations from Meteosat-8.

different reanalysis data sets when compared with observations. As can be seen from Figure 5a, the observed monthly mean BTs in 2015–2017 mainly range from 239 to 261 K. The shape of the PDF of BTs from reanalyses is close to that from observations, but with a leftward shift in position, suggesting an overall cold bias of approximately 2 K. Except for MERRA-2, all reanalysis data sets are close to each other, which is consistent with Figures 2a and 2b. As for the BTDs, JRA55 and CRA have the highest probability of BTDs at -1.75 K while the BTDs in ERA-Interim and CFSR peak at -2.25 K. The highest probability of

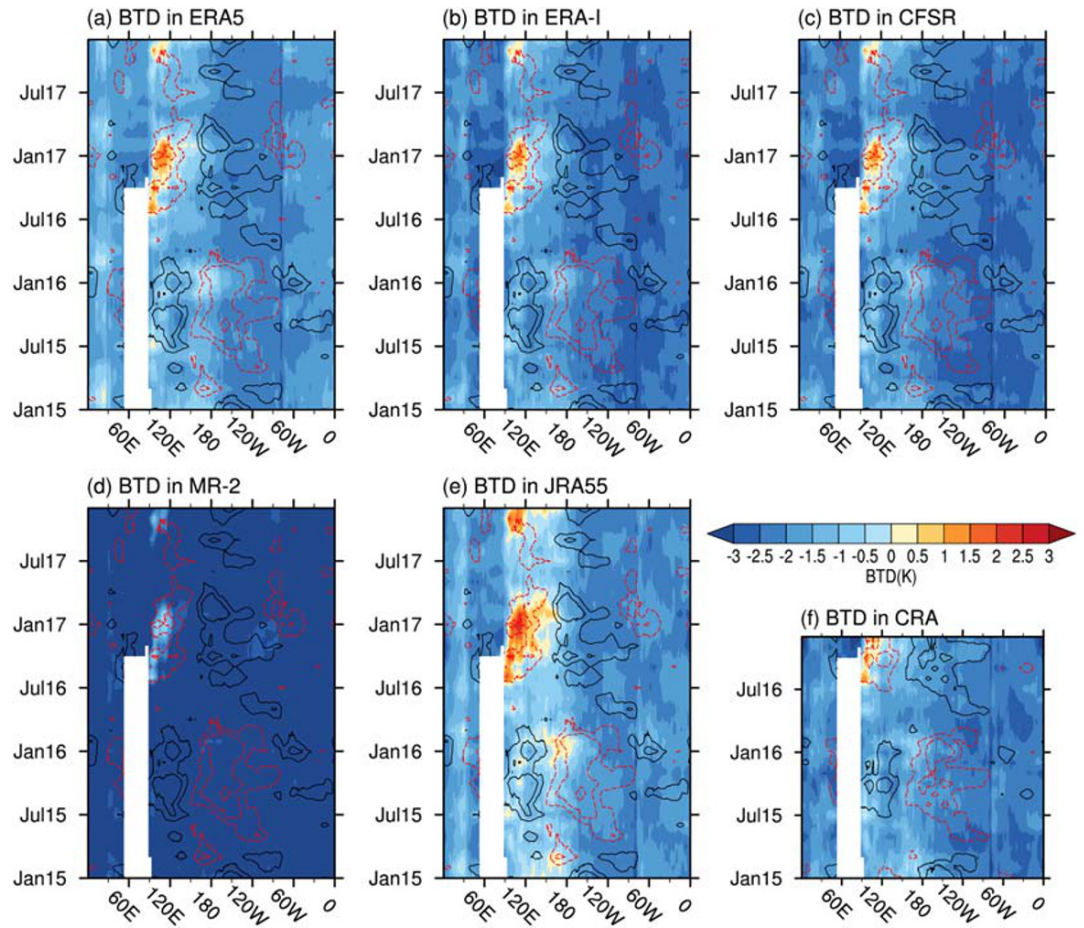


Figure 7. Same as Figure 6, but for (shaded) BTDs and the contours overlaid are BT anomalies from observations in Figure 6a.

BTDs in ERA5 is between -1.75 and -2.25 K. In contrast, the BTDs in MERRA-2 are more decentralized distributed with larger probability of BTD values from -4.5 to -2 K. The PDF scores in Figure 5c provide a quantitative way to assess the similarities between observations and different reanalysis data sets based on the PDF of each data set. Results show that JRA55, CRA, and ERA5 are closer to observations while MERRA-2 is less competitive with the other reanalysis data sets with the skill score of less than 0.7. Additionally, the PDF skill score of ERA5 is slightly larger than that of ERA-Interim, indicating slight improvement in the simulations of UTWV in ERA5 in comparison to ERA-Interim.

3.3. Variation of UTWV During the ENSO Event

The mean distribution of UTWV is an indicator of large-scale atmospheric circulations. Previous studies also found that the upper tropospheric moisture is highly correlated with ENSO events (Shi & Bates, 2011; Shi et al., 2018). Since there is a strong El Niño in the study period, it is valuable to take the chance to assess the simulation of UTWV related with this climate event in reanalysis data sets. This El Niño starts developing in 2015, peaks in the winter of 2015–2016, and decays in the next year of 2016–2017. It is one of the strongest El Niño events on record (Jacox et al., 2016; Shi et al., 2018).

Figure 6 shows the Hovmöller diagrams of the monthly mean BTs with superimposed contours indicating the monthly anomalies of BTs averaged over the equatorial band from 5°N to 5°S , where the signal of ENSO is strongest, in the observed and reanalysis data sets for 2015–2017. The monthly anomalies were calculated by subtracting the long-term (3-year) monthly mean from monthly data at each point from each data set and thus can be used to indicate the evolution of the UTWV signal. Positive (negative) BT anomalies represent the dry (wet) anomalies in the upper troposphere. The distribution of UTWV in the equatorial

region is highly indicative of the ascending and descending branches of the Walker circulation. Over the Pacific, there is a strong low-pressure system with updrafts over the western Pacific and maritime continent ($\sim 120^{\circ}\text{E}$) and a strong high-pressure system with downdrafts in the eastern Pacific ($\sim 120^{\circ}\text{W}$) in the generalized Walker circulation. The rising air brings sufficient moisture to the upper troposphere and forms a cold BT band in the western Pacific. In contrast, the strong descending branches with dry and stable air are located in the eastern Pacific. Similarly, the secondary circulation cells of Walker circulation are also shown with ascending air over land regions of South America ($\sim 60^{\circ}\text{W}$) and Africa ($\sim 25^{\circ}\text{E}$) and compensating descending air over the Atlantic ($\sim 0^{\circ}$) and the Indian Ocean ($\sim 60^{\circ}\text{E}$). The spatial distribution of observed BTs is well captured in reanalysis data sets, but with different magnitudes. The wet band is stronger and the dry band is weaker in reanalysis data sets when compared with observations. In 2015, when the strong El Niño is developing, a cold BT band corresponding to high UTWV in the western Pacific ($\sim 120^{\circ}\text{E}$) starts to propagate eastward indicated by the collocated red arrow in Figure 6a which is determined by the centers of negative BT (wet) anomalies. Meanwhile, the western Pacific is getting drier in the upper troposphere than normal years (positive anomalies). Overall, all reanalysis data sets simulate the observed temporal variabilities very well with dry anomalies over western Pacific and wet anomalies propagating eastward during the developing of the 2015–2016 El Niño. However, reanalyses tend to produce a colder result in the eastern Pacific and with convection (cold BTs) a little further east than observed. After the strong 2015–2016 El Niño, BT anomalies get reversed from June, July, and August (JJA) 2016 with negative anomalies over the western Pacific and positive anomalies to the east, suggesting a transition of this El Niño to a neutral phase or even to a weak cold phase of ENSO.

The moist bias is found throughout most of the tropics in all six reanalysis data sets in Figure 7. The BT anomalies from observations (Figure 6a) are also overlaid to provide the structure of the evolution of the dry/wet signals. Coinciding with findings from Figure 4, the larger negative BT biases are mainly found in the corresponding dry regions in Figure 6 whereas the smaller biases are usually in the wet regions. The most distinct feature is that there is a dry bias (or less moist bias for MERRA-2) first appearing in boreal summer (JJA) of 2016, sustaining and enhancing in winter, and reappearing in the following fall to winter to a far less extent. This dry bias is collocated with the center of observed wet anomalies and moves coherently eastward with the deep convections over the Indo-Pacific warm pool, indicating a modulation by the Madden-Julian oscillation (MJO) (Schreck et al., 2013). The dry bias is most obvious in JRA55 with maxima of 1.5 K and expressed as a smaller wet bias in MERRA-2. This also explains the larger temporal variation of BTDs found in this region highlighted by black stipples in Figure 3. These results indicate that reanalysis data sets tend to underestimate the UTWV in strong convection regions, except MERRA-2, which still overestimates UTWV but to a lesser extent than it does in other regions. Previous studies have also found that the model humidity field is slightly dry in areas associated with deep convection and suggested that the insufficient model convective parameterization might be the underlying cause (Iacono et al., 2003; Luo et al., 2008; Schmetz & van de Berg, 1994; Takahashi et al., 2016). As indicated by the overlaid observed BT anomalies, reanalyses are wetter than observations over the whole equatorial Pacific during the development of this El Niño from mid-2015 to early 2016. In comparison, reanalysis data sets are too moist over the eastern Pacific and too dry over the western Pacific during the dissipation of this El Niño from mid-2016 to early 2017.

The mature phase of El Niño usually occurs in the boreal winter season (December, January, and February [DJF]), and its delayed effect in the next winter is also noteworthy (Kumar & Hoerling, 2003; Ren et al., 2017; Shi et al., 2018). Figures 8 and 9 provide global distributions of the BTs in the mature winter (DJF, 2015–2016) and the next winter (DJF, 2016–2017) of this mature El Niño from observations and reanalysis. The October, November, and December (OND) in 2016 are taken as the next winter in CRA due to the data availability. One significant feature in the El Niño winter is that a narrow cold BT band (colder than ~ 246 K, indicated by the black box in the mature winter of observations) indicative of high UTWV progressed eastward across the Pacific from $\sim 120^{\circ}\text{E}$ to the central and eastern Pacific around 150°W , which is consistent with the findings in Figure 6. Another striking feature is that the warm BT bands over both south and north sides are enhanced, especially the one in the northern Pacific caused by the compensating subsidence of the El Niño convection centered in the equatorial central Pacific. This points to a distinct contrast between dry and wet regions in the mature El Niño winter. In comparison, the eastward propagation in reanalysis data is more obvious with the cold BT band (colder than ~ 246 K) extending to the east end of the equatorial Pacific. However, the magnitude of the drying process over the central northern Pacific is widely underestimated

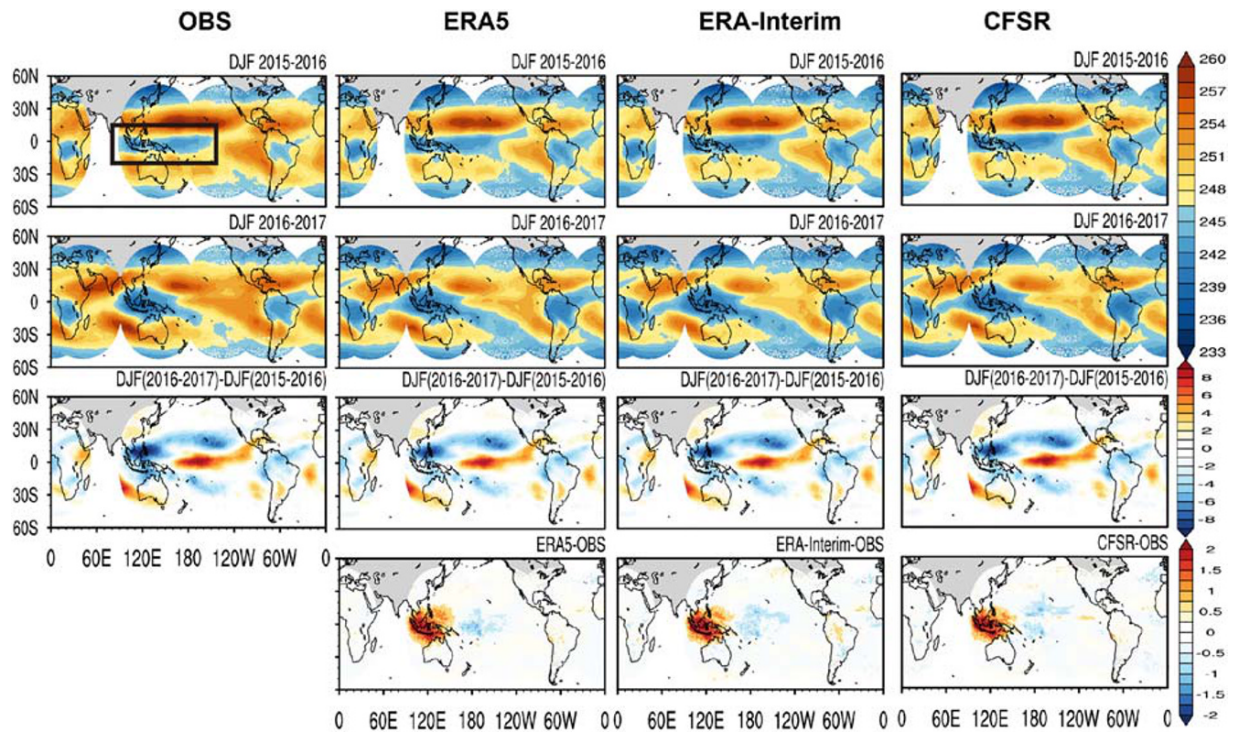


Figure 8. The global distributions of seasonal mean BTs in the (first row) mature winter (DJF 2015–2016), the (second row) next winter (DJF 2016–2017) of this El Niño, the (third row) temporal variation of the BTs in the two winters (next winter minus mature winter), and the (fourth row) differences of the BT temporal variation patterns between reanalysis and observations (reanalysis minus observations). The reanalysis data sets are ERA5, ERA-Interim, and CFSR.

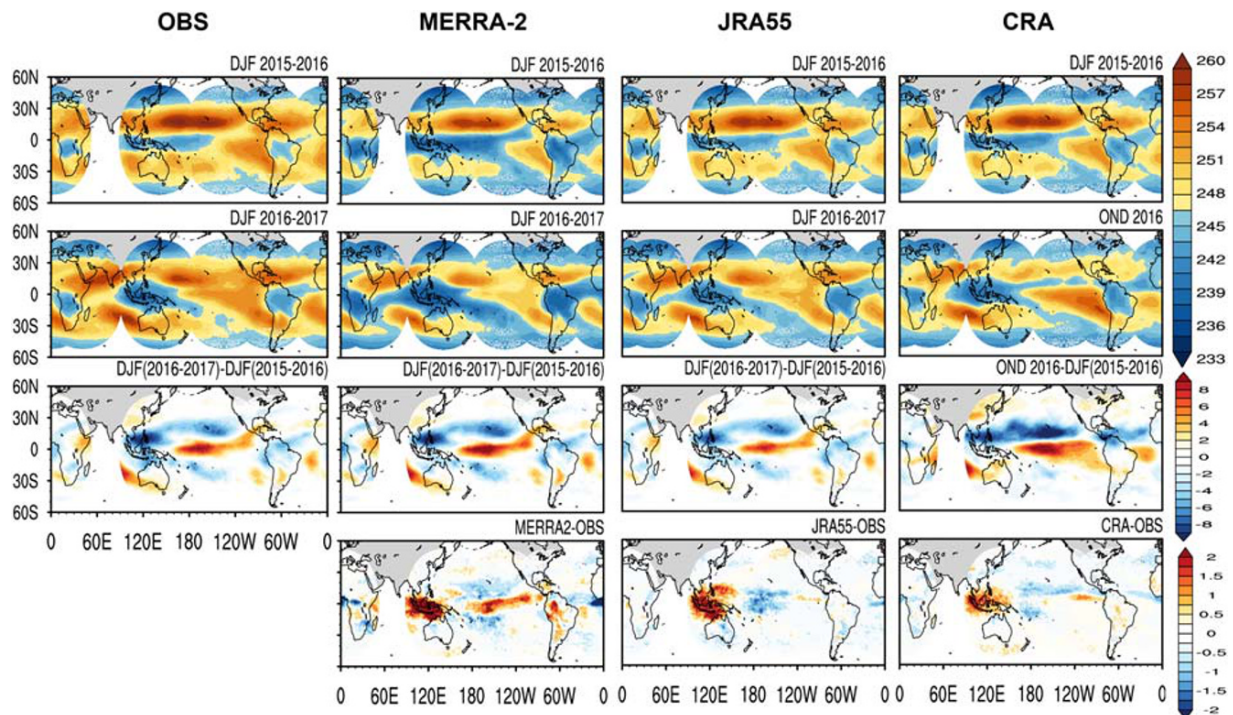


Figure 9. Same as Figure 8, but the reanalysis data sets are MERRA-2, JRA55, and CRA, respectively. Note that the next winter season (OND) in CRA is represented by three different months from other reanalyses.

in reanalysis data sets. In the next winter following the strong El Niño, the Walker circulation returned to the normal phase with the ascending branch back to the maritime continent and the dry descending air over the eastern Pacific. It is shown that the WV accumulated in the upper troposphere again over the western Pacific, and the compensating dry centers over the central northern Pacific weakened and retreated westward. While the dry band over the tropical eastern Pacific enhanced and stretched westward. This transition is also captured in all reanalysis data sets.

The temporal variation of BTs in this process is also shown in the third rows of Figures 8 and 9, which is calculated as BTs in the next winter minus BTs in the mature winter. It is indicative of the UTWV variation in response to the evolution of ENSO in each data set. Consistent with what we mentioned above, the central and eastern Pacific get drier (warmer) coupled with moistening process (colder) to the west over the western Pacific, including the maritime continent, and east over equatorial South America. There are also two bands with opposite variation (moistening) to the north and south of the drying band over the subtropical Pacific from 10–30°N and 10–30°S. This pattern indicates that the BT (or UTWV) field is related to changes in both ascending and descending branches of large-scale circulations and can be used to monitor and diagnose the variation of large-scale circulations. Overall, all reanalysis data sets capture these spatial-temporal variations quite well. However, some discrepancies are revealed by making the differences between the temporal variation patterns of simulations and observations (former minus latter), shown at the bottom rows of Figures 8 and 9. The temporal variation of BTs in the decay year in most reanalysis data sets is underestimated with a strong dry bias in the moistening western Pacific and a wet bias in the drying central Pacific. This underprediction of the gradient between the ascending and descending regions over the tropical Pacific suggests a weakened Walker circulation simulated in reanalysis data sets in the next winter following the 2015–2016 El Niño which should be of a neutral phase or weak La Niña. Although the temporal variation is also underestimated in the western Pacific in MERRA-2, the variation pattern in the central and eastern Pacific is overestimated with an even drier bias in the region extending to eastern Pacific and a wet bias over both the north and south moistening regions. It is noteworthy that the dominant dry bias over the far western Pacific in all reanalyses is also consistent with that identified in Figure 7.

4. Conclusions and Discussions

The UTWV simulated in six modern reanalysis data sets that are widely used for climate studies is evaluated over the period of 2015–2017 using homogenized 6.5- μm WV radiances data from international GEO weather satellites for the first time. Analysis is based on the monthly mean UTWV to demonstrate the feasibility of using GEO satellite observations for climate studies. Since UTWV is one of the less well-measured atmospheric variables, these observational data are very valuable with its higher spatiotemporal resolution and accuracy. To avoid the error caused by retrievals, this study adopted a novel approach to directly compare observations and reanalyses on the radiance level.

Overall, six reanalysis data sets perform well in comparison with observations. This is expected because these reanalysis data sets have assimilated various satellite observations by using enhanced DA systems, which are reported to have larger improvement on forecasts (Klinker et al., 2000). Nonetheless, all reanalysis data sets show a cold BT bias of -1.5 to -3.5 K compared with observations on a near global scale. These cold BT biases correspond to a relative moist error of 25% to 85% in the upper troposphere. Results also show that these larger cold BT biases are dominant over the large-scale subsidence zones where the BTs are larger than 245 K. This probably indicates that models in reanalysis data sets tend to underestimate the intensity of large-scale descending branches. The PDF analysis shows that observed BTs are mainly in the range of 239–261 K. All reanalysis data sets are very close to each other and can reproduce the shape of the observed PDF but with a near -2 K of cold bias, except for MERRA-2, which has larger cold bias and the PDF of which is more spread out. A rating of these reanalysis data sets is also given based on the PDF skill score. It suggests that ERA5, JRA55, and CRA are closer to observations, followed by CFSR and ERA-Interim, while MERRA-2 has the largest deviation.

The study period includes a strong El Niño, which allows the comparison under a more complicated climate condition. Results indicate that the variation of the BT (or UTWV) field is highly related to the changes in both ascending and descending branches of large-scale circulations. It is shown that reanalysis data sets can capture the eastward propagation of the high UTWV from the maritime continent and western

Pacific and the abnormally strong dry band caused by the compensating subsidence of the tropical convection over the subtropical northern Pacific during the developing period of El Niño. Moreover, the following transition of the phase of this ENSO event can also be roughly simulated. However, when compared with observations, reanalysis data sets simulate higher UTWV over the whole equatorial Pacific during the strong El Niño from mid-2015 to early 2016. In contrast, they tend to underestimate the UTWV gradient by producing a strong dry bias in the moistening western Pacific including maritime continent and a wet bias in the drying central Pacific in the decay year, which may suggest a weakened Walker circulation simulated in reanalysis data sets when the observed El Niño is returned to the neutral phase or even to a weak La Niña.

There are some possible causes of these deficiencies found in reanalysis data sets. First, the forecast models used in the reanalysis systems are different. The cloud and convective parametrization used in models could contribute to the differences (Davis et al., 2017; Fujiwara et al., 2017). It is noted that the rain and snow re-evaporation was intentionally increased in MERRA-2 to strengthen the stationary wave and the boreal winter circulation pattern. However, this may lead to a wetter upper troposphere (Molod et al., 2015), and it is also shown in this study that the wet bias from MERRA-2 is more pronounced than in other reanalysis data sets. Moreover, this study implies that the dynamical scheme related to large-scale circulation, especially the descending branches, could be an underlying cause of the upper troposphere moist bias. Second, the DA systems used in current reanalyses are different, and they have different strategies to calculate the assimilation increment. Moreover, there is a variety of assimilated data sources. The quality and availability of input observations have significant impacts on the performance of reanalyses. All these factors may contribute to the overall discrepancies in UTWV simulations in current reanalysis systems. Although it appears difficult to identify the specific causes, it is believed that the improvement of DA systems may help further reduce the differences (Fujiwara et al., 2017; Gelaro et al., 2017; Kobayashi et al., 2015).

GEO satellite observations have wider applications than monitoring current weather, such as the evaluation of UTWV in reanalysis on climate scales, as was shown in this study. From this assessment, the user community gains information on the performance of UTWV simulations in different reanalysis data sets. It will also provide feedback to the modeling and DA community for potential deficiencies and improvements of reanalysis data sets in the future. It is well known that the GEO weather satellite observations are valuable for diurnal analysis attributed to their high temporal resolution (Chung et al., 2009, 2013; Soden, 2000). Interested readers are referred to Xue et al. (2020) for studies of using this new homogenized WV radiances data set to evaluate the diurnal variations of upper tropospheric moisture simulated in different reanalysis data sets.

It should be noted that the WV bands onboard the new generation of international GEO satellites (U.S. GOES-R series, Japanese Himawari-8/-9, Korean GEO-KOMPSAT-2, Chinese FengYun-4 series, and later European MTG series) provide every 10-min operational radiance measurements with 2-km spatial resolution since September 2015 for full disk coverage. For the first time, scientists are able to validate the tropospheric moisture diurnal characteristics of climate reanalysis near globally with multiple WV bands radiance measurements (three bands for USA's GOES, Schmit et al., 2017, 2005, and Japan's Himawari, and two bands for the Advanced Geosynchronous Radiation Imager onboard China's FengYun-4 and the Flexible Combined Imager onboard Europe's Meteosat Third Generation). The homogenization of WV band radiances from the new generation of international GEO weather satellites is needed for future climate applications.

Data Availability Statement

The homogenized WV radiances data from international GEO imagers can be obtained by applying the regression coefficients with the Matlab reader (<https://minds.wisconsin.edu/handle/1793/80454>) to the L1b radiance measurements available from Data Center of Space Science and Engineering Center at University of Wisconsin-Madison (<http://inventory.ssec.wisc.edu/inventory/>). ERA5 and ERA-Interim data are obtained from ECMWF (at <https://www.ecmwf.int/en/forecasts/datasets/browse-reanalysis-datasets>). CFSR and MERRA-2 reanalysis are obtained from <https://rda.ucar.edu/datasets/ds094.0/> and <https://disc.gsfc.nasa.gov/>, respectively. JRA55 reanalysis project carried out by JMA is available online (at <https://rda.ucar.edu/datasets/ds628.0/>). CRA data set is provided by the National Meteorological Information Center of CMA (http://data.cma.cn/data/cdcdetail/dataCode/NAFP_CRA40_FTM_6HOR.html).

Acknowledgments

This work is partly supported by China Scholarship Council (CSC) (Yunheng Xue) and National Key R&D Program 2018YFB0504900 (Di Di). It is also partially supported by NOAA's GOES-R series science program NA15NES4320001 (Mathew Gunshor, Zhonglong Li, Jun Li, Szuchia L. Moeller, and Timothy J. Schmit). The views, opinions, and findings contained in this report are those of the authors and should not be construed as an official NOAA's or U.S. government's position, policy, or decision.

References

Allan, R. P. (2012). The role of water vapour in Earth's energy flows. *Surveys in Geophysics*, 33(3–4), 557–564.

Basha, G., Ratnam, M. V., & Murthy, B. V. K. (2013). Upper tropospheric water vapour variability over tropical latitudes observed using radiosonde and satellite measurements. *Journal of Earth System Science*, 122(6), 1583–1591. <https://doi.org/10.1007/s12040-013-0367-y>

Bates, J. J., & Jackson, D. L. (1997). A comparison of water vapor observations with AMIP1 simulations. *Journal of Geophysical Research*, 102(D18), 21,837–21,852.

Brogniez, H., & Pierrehumbert, R. T. (2006). Using microwave observations to assess large-scale control of free tropospheric water vapor in the mid-latitudes. *Geophysical Research Letters*, 33, L14801. <https://doi.org/10.1029/2006GL026240>

Brogniez, H., Roca, R., & Picon, L. (2006). A clear-sky radiance archive from Meteosat “water vapor” observations. *Journal of Geophysical Research*, 111, D21109. <https://doi.org/10.1029/2006JD007238>

Chuang, H., Huang, X., & Minschwaner, K. (2010). Interannual variations of tropical upper tropospheric humidity and tropical rainy-region SST: Comparisons between models, reanalyses, and observations. *Journal of Geophysical Research*, 115, D21125. <https://doi.org/10.1029/2010JD014205>

Chung, E. S., Soden, B. J., Sohn, B. J., & Schmetz, J. (2011). Model-simulated humidity bias in the upper troposphere and its relation to the large-scale circulation. *Journal of Geophysical Research*, 116, D10110. <https://doi.org/10.1029/2011JD015609>

Chung, E. S., Soden, B. J., Sohn, B. J., & Schmetz, J. (2013). An assessment of the diurnal variation of upper tropospheric humidity in reanalysis data sets. *Journal of Geophysical Research: Atmospheres*, 118, 3425–3430. <https://doi.org/10.1002/jgrd.50345>

Chung, E. S., Sohn, B. J., & Schmetz, J. (2009). Diurnal variation of outgoing longwave radiation associated with high cloud and UTH changes from Meteosat-5 measurements. *Meteorology and Atmospheric Physics*, 105(3–4), 109–119.

Davis, S. M., Hegglin, M. I., Fujiwara, M., Dragani, R., Harada, Y., Kobayashi, C., et al. (2017). Assessment of upper tropospheric and stratospheric water vapor and ozone in reanalyses as part of S-RIP. *Atmospheric Chemistry and Physics*, 17(20), 12,743–12,778. <https://doi.org/10.5194/acp-17-12743-2017>

Dee, D. P., Uppala, S. M., Simmons, A. J., Berrisford, P., Poli, P., Kobayashi, S., et al. (2011). The ERA-Interim reanalysis: Configuration and performance of the data assimilation system. *Quarterly Journal of the Royal Meteorological Society*, 137(656), 553–597. <https://doi.org/10.1002/qj.828>

Dessler, A. E., & Davis, S. M. (2010). Trends in tropospheric humidity from reanalysis systems. *Journal of Geophysical Research*, 115, D19127. <https://doi.org/10.1029/2010JD014192>

Di, D., Ai, Y., Li, J., Shi, W., & Lu, N. (2016). Geostationary satellite-based 6.7 μm band best water vapor information layer analysis over the Tibetan Plateau. *Journal of Geophysical Research: Atmospheres*, 121, 4600–4613. <https://doi.org/10.1002/2016JD024867>

Elliott, W. P., & Gaffen, D. J. (1991). On the utility of radiosonde humidity archives for climate studies. *Bulletin of the American Meteorological Society*, 72(10), 1507–1520.

Fujiwara, M., Wright, J. S., Manney, G. L., Gray, L. J., Anstey, J., Birner, T., et al. (2017). Introduction to the SPARC Reanalysis Intercomparison Project (S-RIP) and overview of the reanalysis systems. *Atmospheric Chemistry and Physics*, 17(2), 1417–1452. <https://doi.org/10.5194/acp-17-1417-2017>

Gelaro, R., McCarty, W., Suárez, M. J., Todling, R., Molod, A., Takacs, L., et al. (2017). The modern-era retrospective analysis for research and applications, version 2 (MERRA-2). *Journal of Climate*, 30(14), 5419–5454. <https://doi.org/10.1175/JCLI-D-16-0758.1>

Gregory, D. (1997). Sensitivity of general circulation model performance to convective parameterization. In *The physics and parameterization of moist atmospheric convection* (pp. 463–482). Dordrecht: Springer.

Han, Y. (2006). JCSDA Community Radiative Transfer Model (CRTM): Version 1.

Held, I. M., & Soden, B. J. (2000). Water vapor feedback and global warming. *Annual Review of Energy and the Environment*, 25(1), 441–475.

Hersbach, H., & Dee, D. (2016). ERA5 reanalysis is in production. *ECMWF Newsletter*, 147(7), 5–6.

Houghton, J. T., Ding, Y. D. J. G., Griggs, D. J., Noguer, M., van der Linden, P. J., Dai, X., et al. (2001). *Climate change 2001: The scientific basis*. Cambridge, UK: The Press Syndicate of the University of Cambridge.

Iacono, M. J., Delamere, J. S., Mlawer, E. J., & Clough, S. A. (2003). Evaluation of upper tropospheric water vapor in the NCAR Community Climate Model (CCM3) using modeled and observed HIRS radiances. *Journal of Geophysical Research*, 108(D2), 4037. <https://doi.org/10.1029/2002JD002539>

Jacox, M. G., Hazen, E. L., Zaba, K. D., Rudnick, D. L., Edwards, C. A., Moore, A. M., & Bograd, S. J. (2016). Impacts of the 2015–2016 El Niño on the California Current System: Early assessment and comparison to past events. *Geophysical Research Letters*, 43, 7072–7080. <https://doi.org/10.1002/2016GL069716>

Jiang, J. H., Su, H., Zhai, C., Wu, L., Minschwaner, K., Molod, A. M., & Tompkins, A. M. (2015). An assessment of upper troposphere and lower stratosphere water vapor in MERRA, MERRA2, and ECMWF reanalyses using Aura MLS observations. *Journal of Geophysical Research: Atmospheres*, 120, 11,468–11,485. <https://doi.org/10.1002/2015JD023752>

Jiang, L., Liu, Z., & Shi, C. (2018). CMA global reanalysis: Status and plans. *AGUFM*, 2018, A11D-06.

John, V. O., & Soden, B. J. (2007). Temperature and humidity biases in global climate models and their impact on climate feedbacks. *Geophysical Research Letters*, 34, L18704. <https://doi.org/10.1029/2007GL030429>

Klinker, E., Rabier, F., Kelly, G., & Mahfouf, J.-F. (2000). The ECMWF operational implementation of four-dimensional variational assimilation. III: Experimental results and diagnostics with operational configuration. *Quarterly Journal of the Royal Meteorological Society*, 126(564), 1191–1215. <https://doi.org/10.1002/qj.49712656417>

Kobayashi, S., Ota, Y., Harada, Y., Ebata, A., Moriya, M., Onoda, H., et al. (2015). The JRA-55 reanalysis: General specifications and basic characteristics. *Journal of the Meteorological Society of Japan Series II*, 93(1), 5–48. <https://doi.org/10.2151/jmsj.2015-001>

Kumar, A., & Hoerling, M. P. (2003). The nature and causes for the delayed atmospheric response to El Niño. *Journal of Climate*, 16(9), 1391–1403.

Lavers, D. A., Ralph, F. M., Waliser, D. E., Gershunov, A., & Dettinger, M. D. (2015). Climate change intensification of horizontal water vapor transport in CMIP5. *Geophysical Research Letters*, 42, 5617–5625. <https://doi.org/10.1002/2015GL064672>

Li, Z., Li, J., Gunshor, M., Moeller, S. C., Schmit, T. J., Yu, F., & McCarty, W. (2019). Homogenized water vapor absorption band radiances from international geostationary satellites. *Geophysical Research Letters*, 46, 10,599–10,608. <https://doi.org/10.1029/2019GL083639>

Luo, Z., Kley, D., Johnson, R. H., & Smit, H. (2008). Ten years of measurements of tropical upper-tropospheric water vapor by MOZAIC. Part II: Assessing the ECMWF humidity analysis. *Journal of Climate*, 21(7), 1449–1466.

Mao, J., Shi, X., Ma, L., Kaiser, D. P., Li, Q., & Thornton, P. E. (2010). Assessment of reanalysis daily extreme temperatures with China's homogenized historical dataset during 1979–2001 using probability density functions. *Journal of Climate*, 23(24), 6605–6623.

- Maxino, C. C., McAvaney, B. J., Pitman, A. J., & Perkins, S. E. (2008). Ranking the AR4 climate models over the Murray-Darling Basin using simulated maximum temperature, minimum temperature and precipitation. *International Journal of Climatology*, *28*(8), 1097–1112. <https://doi.org/10.1002/joc.1612>
- Menzel, W. P., Schmit, T. J., Zhang, P., & Li, J. (2018). Satellite-based atmospheric infrared sounder development and applications. *Bulletin of the American Meteorological Society*, *99*(3), 583–603.
- Miloshevich, L. M., Vömel, H., Whiteman, D. N., Lesht, B. M., Schmidlin, F. J., & Russo, F. (2006). Absolute accuracy of water vapor measurements from six operational radiosonde types launched during AWEX-G and implications for AIRS validation. *Journal of Geophysical Research*, *111*, D09S10. <https://doi.org/10.1029/2005JD006083>
- Molod, A., Takacs, L., Suarez, M., & Bacmeister, J. (2015). Development of the GEOS-5 atmospheric general circulation model: Evolution from MERRA to MERRA2. *Geoscientific Model Development*, *8*(5), 1339–1356. <https://doi.org/10.5194/gmd-8-1339-2015>
- Pierce, D. W., Barnett, T. P., Fetzner, E. J., & Gleckler, P. J. (2006). Three-dimensional tropospheric water vapor in coupled climate models compared with observations from the AIRS satellite system. *Geophysical Research Letters*, *33*, L21701. <https://doi.org/10.1029/2006GL027060>
- Ren, R., Rao, J., Wu, G., & Cai, M. (2017). Tracking the delayed response of the northern winter stratosphere to ENSO using multi reanalyses and model simulations. *Climate Dynamics*, *48*(9), 2859–2879. <https://doi.org/10.1007/s00382-016-3238-9>
- Saha, S., Moorthi, S., Wu, X., Wang, J., Nadiga, S., Tripp, P., et al. (2014). The NCEP climate forecast system version 2. *Journal of Climate*, *27*(6), 2185–2208. <https://doi.org/10.1175/JCLI-D-12-00823.1>
- Santer, B. D., Sausen, R., Wigley, T. M. L., Boyle, J. S., AchutaRao, K., Doutriaux, C., et al. (2003). Behavior of tropopause height and atmospheric temperature in models, reanalyses, and observations: Decadal changes. *Journal of Geophysical Research*, *108*(D1), 4002. <https://doi.org/10.1029/2002JD002258>
- Schmetz, J., Gejo, C., Menzel, W. P., Strabala, K., Van De Berg, L., Holmlund, K., & Tjemkes, S. (1995). Satellite observations of upper tropospheric relative humidity, clouds and wind field divergence. *Contributions to Atmospheric Physics/Beitraege zur Physik der Atmosphaere*, *68*(4), 345–357.
- Schmetz, J., Menzel, W. P., Velden, C., Wu, X., van de Berg, L., Nieman, S., et al. (1995). Monthly mean large-scale analyses of upper-tropospheric humidity and wind field divergence derived from three geostationary satellites. *Bulletin of the American Meteorological Society*, *76*(9), 1578–1584. [https://doi.org/10.1175/1520-0477\(1995\)076<1578:MMLSAO>2.0.CO;2](https://doi.org/10.1175/1520-0477(1995)076<1578:MMLSAO>2.0.CO;2)
- Schmetz, J., & van de Berg, L. (1994). Upper tropospheric humidity observations from Meteosat compared with short-term forecast fields. *Geophysical Research Letters*, *21*(7), 573–576.
- Schmit, T. J., Griffith, P., Gunshor, M. M., Daniels, J. M., Goodman, S. J., & Lebair, W. J. (2017). A closer look at the ABI on the GOES-R series. *Bulletin of the American Meteorological Society*, *98*(4), 681–698.
- Schmit, T. J., Gunshor, M. M., Menzel, W. P., Gurka, J. J., Li, J., & Bachmeier, A. S. (2005). Introducing the next-generation Advanced Baseline Imager on GOES-R. *Bulletin of the American Meteorological Society*, *86*(8), 1079–1096.
- Schreck, C. J. III, Shi, L., Kossin, J. P., & Bates, J. J. (2013). Identifying the MJO, equatorial waves, and their impacts using 32 years of HIRS upper-tropospheric water vapor. *Journal of Climate*, *26*(4), 1418–1431.
- Shangguan, M., Wang, W., & Jin, S. (2019). Variability of temperature and ozone in the upper troposphere and lower stratosphere from multi-satellite observations and reanalysis data. *Atmospheric Chemistry and Physics*, *19*(10), 6659–6679. <https://doi.org/10.5194/acp-19-6659-2019>
- Shi, L., & Bates, J. J. (2011). Three decades of intersatellite-calibrated High-Resolution Infrared Radiation Sounder upper tropospheric water vapor. *Journal of Geophysical Research*, *116*, D04108. <https://doi.org/10.1029/2010JD014847>
- Shi, L., Schreck, C. J., & Schröder, M. (2018). Assessing the pattern differences between satellite-observed upper tropospheric humidity and total column water vapor during major El Niño events. *Remote Sensing*, *10*(8), 1188.
- Soden, B. J. (2000). The diurnal cycle of convection, clouds, and water vapor in the tropical upper troposphere. *Geophysical Research Letters*, *27*(15), 2173–2176.
- Soden, B. J., & Bretherton, F. P. (1993). Upper tropospheric relative humidity from the GOES 6.7 μ m channel: Method and climatology for July 1987. *Journal of Geophysical Research*, *98*(D9), 16,669–16,688.
- Soden, B. J., & Bretherton, F. P. (1994). Evaluation of water vapor distribution in general circulation models using satellite observations. *Journal of Geophysical Research*, *99*(D1), 1187–1210.
- Su, H., Jiang, J. H., Zhai, C., Perun, V. S., Shen, J. T., Del Genio, A., et al. (2013). Diagnosis of regime-dependent cloud simulation errors in CMIP5 models using “A-Train” satellite observations and reanalysis data. *Journal of Geophysical Research: Atmospheres*, *118*, 2762–2780. <https://doi.org/10.1029/2012JD018575>
- Takacs, L. L., Suárez, M. J., & Todling, R. (2016). Maintaining atmospheric mass and water balance in reanalyses. *Quarterly Journal of the Royal Meteorological Society*, *142*(697), 1565–1573. <https://doi.org/10.1002/qj.2763>
- Takahashi, H., Su, H., & Jiang, J. H. (2016). Error analysis of upper tropospheric water vapor in CMIP5 models using “A-Train” satellite observations and reanalysis data. *Climate Dynamics*, *46*(9), 2787–2803. <https://doi.org/10.1007/s00382-015-2732-9>
- Tian, B., Soden, B. J., & Wu, X. (2004). Diurnal cycle of convection, clouds, and water vapor in the tropical upper troposphere: Satellites versus a general circulation model. *Journal of Geophysical Research*, *109*, D10101. <https://doi.org/10.1029/2003JD004117>
- Trenberth, K. E., Fasullo, J. T., & Mackaro, J. (2011). Atmospheric moisture transports from ocean to land and global energy flows in reanalyses. *Journal of Climate*, *24*(18), 4907–4924.
- Trenberth, K. E., Stepaniak, D. P., Hurrell, J. W., & Fiorino, M. (2001). Quality of reanalyses in the tropics. *Journal of Climate*, *14*(7), 1499–1510.
- van de Berg, L., Pyonjamsri, A., & Schmetz, J. (1991). Monthly mean upper tropospheric humidities in cloud-free areas from meteosat observations. *International Journal of Climatology*, *11*(8), 819–826.
- Wang, J., Carlson, D. J., Parsons, D. B., Hock, T. F., Lauritsen, D., Cole, H. L., et al. (2003). Performance of operational radiosonde humidity sensors in direct comparison with a chilled mirror dew-point hygrometer and its climate implication. *Geophysical Research Letters*, *30*(16), 1860. <https://doi.org/10.1029/2003GL016985>
- Xue, Y., Li, J., Li, Z., Gunshor, M. M., & Schmit, T. J. (2020). Evaluation of the diurnal variation of upper tropospheric humidity in reanalysis using homogenized observed radiances from international geostationary weather satellites. *Remote Sensing*, *12*, 1628. <https://doi.org/10.3390/rs12101628>
- Xue, Y., Li, J., Menzel, W. P., Borbas, E., Ho, S. P., Li, Z., & Li, J. (2019). Characteristics of satellite sampling errors in Total Precipitable Water from SSMIS, HIRS, and COSMIC observations. *Journal of Geophysical Research: Atmospheres*, *124*, 6966–6981. <https://doi.org/10.1029/2018JD030045>

Zhan, R., Li, J., & Gettelman, A. (2006). Intraseasonal variations of upper tropospheric water vapor in Asian monsoon region. *Atmospheric Chemistry and Physics Discussions*, 6(4), 8069–8095. <https://doi.org/10.5194/acpd-6-8069-2006>